Electrocatalytic Urea Synthesis via N_2 Dimerization and Universal Descriptor

Junxian Liu[1], Xingshuai Lv[2], Yandong Ma[3], Sean C. Smith[4], Yuantong Gu[1*], and Liangzhi Kou[1*]

[1]School of Mechanical, Medical and Process Engineering, Queensland University of Technology, Brisbane QLD 4001, Australia.

[2]Institute of Applied Physics and Materials Engineering, University of Macau, Macao SAR 999078, China.

[3]School of Physics, State Key Laboratory of Crystal Materials, Shandong University, Shandanan Street 27, Jinan 250100, China.

[4]Integrated Materials Design Laboratory, Department of Materials Physics, Research School of Physics, The Australian National University, Australian Capital Territory, Canberra, ACT 2601, Australia.

Email: yuantong.gu@qut.edu.au, liangzhi.kou@qut.edu.au

ABSTRACT: Electrocatalytic urea synthesis through N_2 + CO_2 co-reduction and C−N coupling is a promising and sustainable alternative to harsh industrial processes. Despite considerable efforts, limited progress has been made due to the challenges of breaking inert N≡N bonds for C−N coupling, competing side reactions, and the absence of theoretical principles guiding catalyst design. In this study, we propose a new mechanism for highly electrocatalytic urea synthesis using two adsorbed N_2 molecules and CO as nitrogen and carbon sources, respectively. This mechanism circumvents the challenging step of N≡N bond breaking and selective CO_2 to CO reduction, as the free CO molecule inserts into dimerized *N_2 and binds concurrently with two N atoms, forming a unique urea precursor *NNCONN* with both thermodynamic and kinetic feasibility. Through the new mechanism, $Ti_2@C_4N_3$ and $V_2@C_4N_3$ are identified as highly active catalysts for electrocatalytic urea formation, exhibiting low onset potentials of -0.741 and -0.738 V, respectively. Importantly, taking transition metal atoms anchored on porous graphite-like carbonitride ($TM_2@C_4N_3$) as prototypes, we introduce a simple descriptor, namely, effective d electron number (Φ), to quantitatively describe the structure-activity relationships for urea formation. This descriptor incorporates inherent atomic properties of the catalyst, such as the number of d electrons, electronegativity of the metal atoms, and generalized electronegativity of the substrate atoms, making it potentially applicable to other urea catalysts. Our work advances novel mechanisms and provides a universal guiding principle for catalyst design in urea electrochemical synthesis.

KEYWORDS: *Electrocatalytic urea synthesis, N_2 dimerization, direct C−N coupling, catalytic descriptor Φ*

1. Introduction

Urea ($CO(NH_2)_2$) is a critically needed fertilizer with nitrogen content up to 46% and an essential nutrition for agricultural crops; the increased grain production due to urea usage plays a vital role in feeding almost 27% of the world's population.[1-2] Urea also holds immense versatility as a raw material in both the chemical and pharmaceutical industries, which is commonly used in topical dermatological products and synthesizing barbiturates, as well as a significant additive in reducing NO_x emissions in the exhaust gases from diesel and lean-burn natural gas engines.[3-7] A sustainable and efficient urea production industry is key to meeting the ever-growing demands of the global population, industrialization, and reduction of environmental pollution. However, the current industrial synthesis of urea is energy-intensive, utilizing harsh conditions (150−200℃, 150−250 bar) and consuming approximately 80% of the global supply of NH_3 produced through artificial N_2 fixation using the Haber-Bosch process,[8-10] which result in substantial greenhouse gas emissions.[11-13] Thus, finding methods to synthesize urea under milder conditions is a highly sought-after and long-awaited development, with the potential to significantly reduce energy consumption and environmental impact.

A highly attractive strategy for achieving mild-condition urea synthesis is through the electrochemical coupling of CO_2 and N_2 at ambient temperature and atmospheric pressure. Recent groundbreaking work by Chen et al. showcased the potential of mild-condition urea production, demonstrating that PdCu particles on TiO_2 sheets could produce urea at a rate of 3.36 mmol/g.h with a Faradic efficiency of 8.92%.[14] This pioneering experimental work has paved the way for further exploration of catalysts such as 2D Mbenes,[15] dual-Si doped carbon nitride,[16] CuB_{12} nanosheet,[17] and frustrated Lewis pairs[18] as potential candidates for urea synthesis. However, the number of reported catalysts remains limited, and their catalytic activity and selectivity are often hindered by intrinsic issues, including the sluggish cleavage of N≡N bonds (with a bond strength of 940.95 kJ/mol)[19] and selective reduction of $CO_2 \rightarrow CO$ to facilitate the subsequent C−N coupling reaction.[18, 20-21] Overcoming these obstacles, such as avoiding N≡N bond breaking and mitigating the occurrence of multiple competing side reactions, is expected to enhance electrocatalytic selectivity and improve urea yields. Furthermore, the scarcity of urea catalysts and their low efficiency are also attributed to the lack of effective theoretical principles guiding catalyst design and a comprehensive understanding of the electrocatalytic

process. Unlike extensively studied processes including hydrogen evolution reaction (HER), oxygen evolution/reduction reaction (OER/ORR), and CO_2 reduction reaction (CO_2RR), where various descriptors such as p/d band centers,[22-25] spin moments,[26-27] charge transfer,[28] or active surface densities[29] are commonly employed for rational catalyst design, the lack of an analogous descriptor for urea synthesis that is capable of simplifying catalyst design and capturing the essence of the reaction, is currently a pressing concern.

In this study, we propose a novel mechanism for electrocatalytic urea production that facilitates the desirable N−C−N bond formation without breaking the inert and stable N≡N bonds, as illustrated in Figure 1a. This mechanism involves the simultaneous chemisorption of two N_2 molecules on bi-active sites with a side-on configuration, recognized as the ideal initiation for adsorbing and activating the inert N_2 molecule. By utilizing dimerized $*N_2$, CO can be embedded into two $*N_2$ molecules to achieve direct and concurrent N−C−N coupling, resulting in the formation of a unique intermediate, namely *NNCONN*. Compared to conventional C−N coupling processes that form the NCON precursor,[14-15, 30-31] the synchronous C−N coupling facilitated by $*N_2$ dimerization and CO eliminates the need for challenging N−N bond rupture and selective reduction of CO_2 to CO. Once *NNCONN* is formed, subsequent hydrogenation processes can generate ammonia and urea.

To verify this proposed mechanism, we conduct the catalytic analysis via density functional theory (DFT) simulations on $TM_2@C_4N_3$ structures, where transition metal (TM) atoms are anchored on porous graphite-like carbonitride (g-C_4N_3). These calculations enable us to construct a simple descriptor Φ (Figure 1b), which assesses the catalytic performance of $TM_2@C_4N_3$ for urea formation. By calculating the adsorption energies for the first and second chemisorption steps ($\Delta E_{*NN-NN*}$ and $\Delta E_{*NNCONN*}$, respectively) over 28 $TM_2@C_4N_3$ structures, a moderate $\Delta E_{*NN-NN*}$ is identified as the prerequisite for a direct C−N coupling reaction. To describe the catalytic performance for urea production and quantify the structure-activity relationships, the descriptor Φ is constructed based on the intrinsic properties of catalysts, which can accurately predict the free energy change (ΔG_L) of the rate-limiting step (RLS) for urea formation eliminating the need for any DFT calculations. Using Φ as the descriptor, $Ti_2@C_4N_3$ and $V_2@C_4N_3$ are identified as promising electrocatalysts capable of

simultaneously activating two N_2 molecules and facilitating the C−N coupling process, exhibiting low onset potentials of -0.741 V ($Ti_2@C_4N_3$) and -0.738 V ($V_2@C_4N_3$) for urea formation.

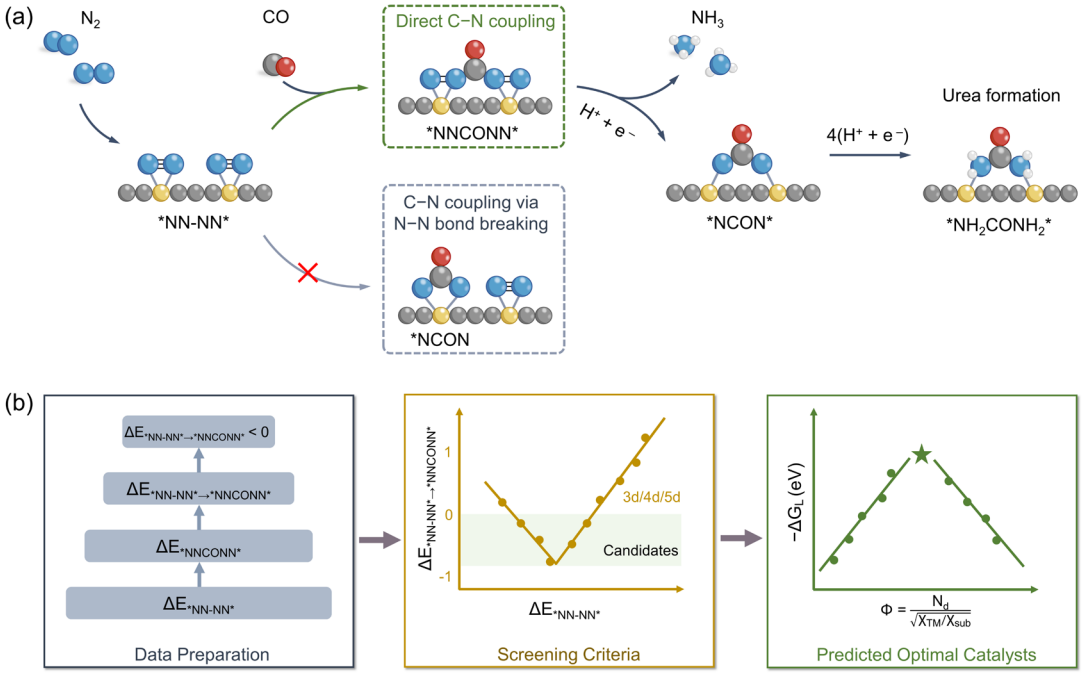

Figure 1. (a) Schematic diagram showing the proposed mechanism for the direct C−N coupling via *NNCONN* intermediate without breaking the N≡N bond for ammonia and urea electrocatalytic synthesis; (b) Workflow for screening highly efficient electrocatalysts for urea formation by the descriptor. (I) Data preparation process. Adsorption energies of dual N_2 molecules ($\Delta E_{*NN-NN*}$) and the *NNCONN* intermediate ($\Delta E_{*NNCONN*}$) on different $TM_2@C_4N_3$ are first calculated to determine the energy changes of $\Delta E_{*NN-NN*\rightarrow*NNCONN*}$. (II) Screening criteria. $TM_2@C_4N_3$ candidates with excellent C−N coupling ($\Delta E_{*NN-NN*\rightarrow*NNCONN*} < 0$) are selected to explore their electrocatalytic urea formation. (III) Descriptor construction process. The characteristics of the catalysts are combined to build the descriptor, and the obtained descriptor is fitted with the ΔG_L of the catalyst.

2. Results and discussions

2.1 New mechanism of electrocatalytic urea synthesis from $2N_2$ + CO

Previous studies have identified the tower-like configuration of *NCON as a key reaction intermediate for the electrochemical urea synthesis.[14-16, 20, 30-31] However, the formation of C−N bonds faces challenges due to the sluggish nature of inserting *CO into the stable N≡N bond, which

necessitates overcoming the strong bond energy of inert N_2 molecules. To solve the problem and increase the reaction efficiency, here we propose a new mechanism for electrochemical urea formation from N_2 and CO. As shown in the Figure 1a, the complete dual-N_2 and CO co-reduction process can be divided into three steps: (1) the adsorption and activation of two N_2 molecules on bi-active sites; (2) the formation of the key *NNCONN* intermediate; and (3) the protonation of *NNCONN* to urea. During the initial step, two N_2 molecules need to be chemisorbed and properly activated with a side-on configuration to form the *NN-NN* species. Subsequently, CO is inserted into two adsorbed N_2 molecules through direct and concurrent C−N coupling, leading to the formation of a *NCON-like intermediate, i.e., *NNCONN*. For the third step, *NNCONN* is reduced to ammonia by removing two side N atoms and then urea through 10 consecutive proton-coupled electron transfer (PCET) steps. In particular, *NNCONN* is attacked by the first two PCET steps, resulting in the formation of *NH_2NCONN* through consecutive pathway. Then, *NH_2NCONN* is further reduced to *NH_2NCONNH_2*, and two NH_3 molecules are released via subsequent protonation steps, leading to the generation of *NCON*. Finally, *NCON* can be further protonated to produce urea (*NH_2CONH_2*).

2.2 Screening of $TM_2@C_4N_3$ for urea synthesis

In our proposed mechanism of urea production as illustrated in Figure 1a, the *N_2 dimerization is believed to be the first prerequisite for an efficient N_2 and CO co-reduction process, where the crucial factor of active sites is the existence of empty orbitals to accept the lone-pair electrons of N_2. Therefore, 28 different TM atoms supported on the g-C_4N_3 substrate are selected as the models for data preparation, as shown in Figure 2a. For these considered $TM_2@C_4N_3$, the co-adsorption energies ($\Delta E_{*NN-NN*}$) of two N_2 molecules via side-on pattern are firstly calculated, as shown in Figures 2b and 2d. It is found that all studied $TM_2@C_4N_3$ catalysts exhibit a pronounced binding affinity towards two N_2 molecules ($\Delta E_{*NN-NN*} < 0$), indicating the ease of N_2 dimerization. Then, the adsorption energies of *NNCONN* on all considered $TM_2@C_4N_3$ catalysts are further calculated, as presented in Figures 2c and 2d. According to the Sabatier principle,[32-33] the catalytic efficiency of a given surface will be maximum when the adsorbate–surface interaction strength reaches the optimal value. Thus, the adsorption strength

of two N_2 molecules on $TM_2@C_4N_3$ cannot be too strong (to over-activate N_2 molecules) or too weak (so that the activation of N_2 molecules is not enough for the following reaction). The adsorption strength will determine the interaction between the dimerized $*N_2$ and CO molecule, thereby affecting the reaction activity of urea production. It is of interest to see a linear relationship between the $\Delta E_{*NN-NN*}$ and $\Delta E_{*NNCONN*}$ (Figure S1), implying a potential inherent correlation between two intermediates. Indeed, Figure 2e reveals that there is a "V shape" bi-linear relationship between $\Delta E_{*NN-NN* \rightarrow *NNCONN*}$ and $\Delta E_{*NN-NN*}$, and the data point located in the valley of this relationship indicates the optimal range of $*N_2$ activations, which can lead to a rapid insertion of CO and a concurrently facile C–N coupling process. For a desired catalyst, the reaction step of *NN-NN* + CO → *NNCONN* is anticipated to be exothermic, resulting from the fully activated N_2 molecules. Based on this screening criterion, 9 $TM_2@C_4N_3$ (TM = Ti, V, Cr, Nb, Mo, Tc, Ta, W, and Re) candidates with $\Delta E_{*NN-NN* \rightarrow *NNCONN*} < 0$, therefore, are singled out for the further activity evaluation, as shown in the Figure 2e and Table S1.

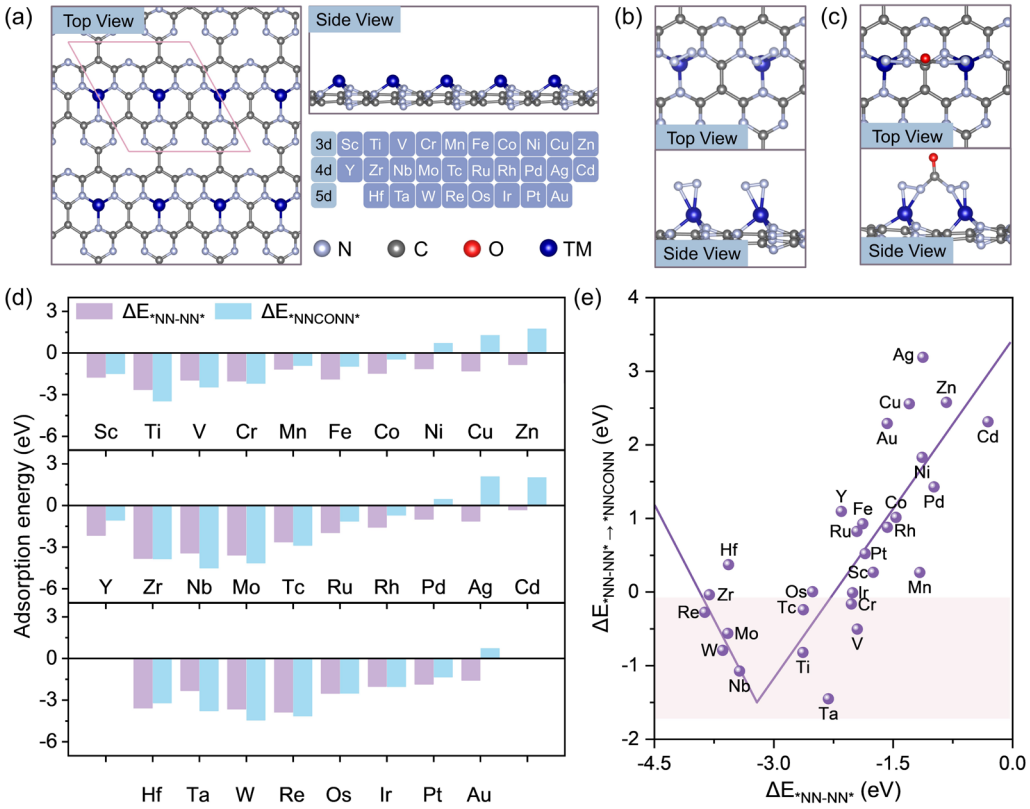

Figure 2. Atomic structures of (a) $TM_2@C_4N_3$ catalysts, (b) dual-N_2 adsorption (*NN-NN*), (c) and *NNCONN* intermediate on $TM_2@C_4N_3$; (d) Calculated adsorption energies of *NN-NN* and *NNCONN* intermediates on $TM_2@C_4N_3$; (e) Fitted relationship between the reaction energy change

of $\Delta E_{*NN-NN*\rightarrow *NNCONN}$ and $\Delta E_{*NN-NN*}$. The highlighted area denotes the possible C−N coupling process ($\Delta E_{*NN-NN*\rightarrow *NNCONN*} < 0$).

To explore the reaction activity for urea formation, further DFT calculations for the entire reduction pathway, involving consecutive PCET steps following Figure 3a, are conducted on the screened $TM_2@C_4N_3$ (TM = Ti, V, Cr, Nb, Mo, Tc, Ta, W, and Re) candidates, as presented in Figures 3b-d and Figures S2-S3. Here, we mainly focus on the discussions on the detailed $2N_2$ + CO co-reduction processes, taking $V_2@C_4N_3$ as a typical example (Figures 3c and S3b). As mentioned above, an effective adsorption of two N_2 molecules on active sites is a prerequisite for subsequent electrochemical reaction. It is indicative that *NN-NN* can be strongly adsorbed on $V_2@C_4N_3$ with a $\Delta G_{*NN-NN*}$ of -0.98 eV, which lays the foundation for the insertion of CO. The pivotal intermediate, referred to as the tower-like *NNCONN*, is then formed through embedding the CO in *NN-NN*, resulting in a small uphill process of 0.315 eV. Afterwards, the intermediate *NNCONN* is attacked by one proton-electron pair, forming the competitive *NHNCONN* or *NNHCONN*. In Table S2, the energies of these two species are summarized for $V_2@C_4N_3$. It can be found that the $E_{*NHNCONN*}$ is more negative compared to that of $E_{*NNHCONN*}$, that is, *NHNCONN* is energetically more favorable than *NNHCONN*, as shown in Figure 3c and Table S2. For the second proton-electron pair transfer, in comparison to the symmetric hydrogenation of *NHNCONNH*, the asymmetric protonation of $*NH_2NCONN*$ is identified as the preferred pathway due to its energetical stability (Table S2). Subsequently, the nitrogen on the other side of $*NH_2NCONN*$ will undergo further attack for the symmetrical protonation, leading to the formation of $*NH_2NCONNH_2*$ after two PCET steps. Once the $*NH_2NCONNH_2*$ intermediate is generated, the formation of NH_3 on $V_2@C_4N_3$ becomes very straightforward. Particularly, there are two different pathways, namely enzymatic and mixed, as depicted in Figure 3a. For $V_2@C_4N_3$, two NH_3 molecules can be exothermically released from the surface through either the enzymatic route: $*NH_2NCONNH_2* \rightarrow *NCONNH_2* \rightarrow *NCON*$, or the mixed route: $*NH_2NCONNH_2* \rightarrow *NCONNH_2* \rightarrow *NHCONNH_2* \rightarrow *NHCON*$. Thereafter, the urea can be formed through the further reduction of the conventional intermediates *NCON* or *NHCON*, where the last hydrogenation step to $*NH_2CONH_2*$ is identified as the potential determining step (PDS) with the ΔG of 0.738 eV, corresponding to the onset potential (U_{Urea}^{onset}) of -0.738 V.

Furthermore, as shown in Figures 3 and S2, our computations indicate that the possible PDS of $2N_2$ + CO co-reduction reaction on $TM_2@C_4N_3$ systems can be from the last two hydrogenated intermediates, namely *NH_2CONH* (*$NHCONH$* + $H^+ + e^- \rightarrow$ *NH_2CONH*) or *NH_2CONH_2* (*NH_2CONH* + $H^+ + e^- \rightarrow$ *NH_2CONH_2*), while the formation of NH_3 is spontaneous through the enzymatic intermediate *$NH_2NCONNH_2$*. Among all screened candidates based on Figure 2e, $TM_2@C_4N_3$ (TM = Cr, Mo, Tc, Ta, and Re) show the low activity for electrocatalytic urea production via $2N_2$ + CO co-reduction, resulting from the large onset potentials of -1.544 V for $Cr_2@C_4N_3$ (*NH_2CONH_2*), -1.310 V for $Mo_2@C_4N_3$ (*NH_2CONH_2*), -1.029 V for $Tc_2@C_4N_3$ (*NH_2CONH_2*), -1.193 V for $Ta_2@C_4N_3$ (*NH_2CONH*), and -1.508 V for $Re_2@C_4N_3$ (*NH_2CONH_2*), respectively. As a comparison, $TM_2@C_4N_3$ (TM = Ti, V, Nb, and W) with the theoretical onset potentials of -0.741 V (*NH_2CONH* for $Ti_2@C_4N_3$), -0.738 V (*NH_2CONH_2* for $V_2@C_4N_3$), -0.754 V (*NH_2CONH* for $Nb_2@C_4N_3$), and -0.745 eV (*NH_2CONH* for $W_2@C_4N_3$), respectively, are screened out as the promising catalysts for electrocatalytic urea formation from N_2 dimerization and CO, which are comparable to the state-of-the-art electrocatalyst (-0.64 V for benchmark PdCu alloy).[14] Due to the fact that urea electrosynthesis takes place in an aqueous solution, we also investigate the solvent effect on the catalytic activity of the $TM_2@C_4N_3$ for urea production. To this end, solvation of the surface and adsorbates is taken into account by using the Poisson–Boltzmann implicit solvation model in VASPsol with the dielectric constant of 78.4 for water.[34-35] Here, our primary focus lies on the $Ti_2@C_4N_3$ and $V_2@C_4N_3$, which exhibit the lowest onset potentials among the screened promising catalyst. By comparing the calculated ΔG values of all the elementary steps of urea synthesis through dimerized *N_2 and CO with and without solvent effects (Figure S4 and Figures 3b-c), it is found that these reaction intermediates are stabilized (such as *$NCONNH_2$*, *NCON*, and *NH_2CONH*) or destabilized (such as *NN-NN*, *NNCONN*, and *$NH_2NCONNH$*) to different degrees. However, it is worth noting that the change in the onset potentials for urea formation on the $Ti_2@C_4N_3$ and $V_2@C_4N_3$ is relatively small (Figure S4), indicating that the solvent effect has a minimal impact on their excellent catalytic performance.

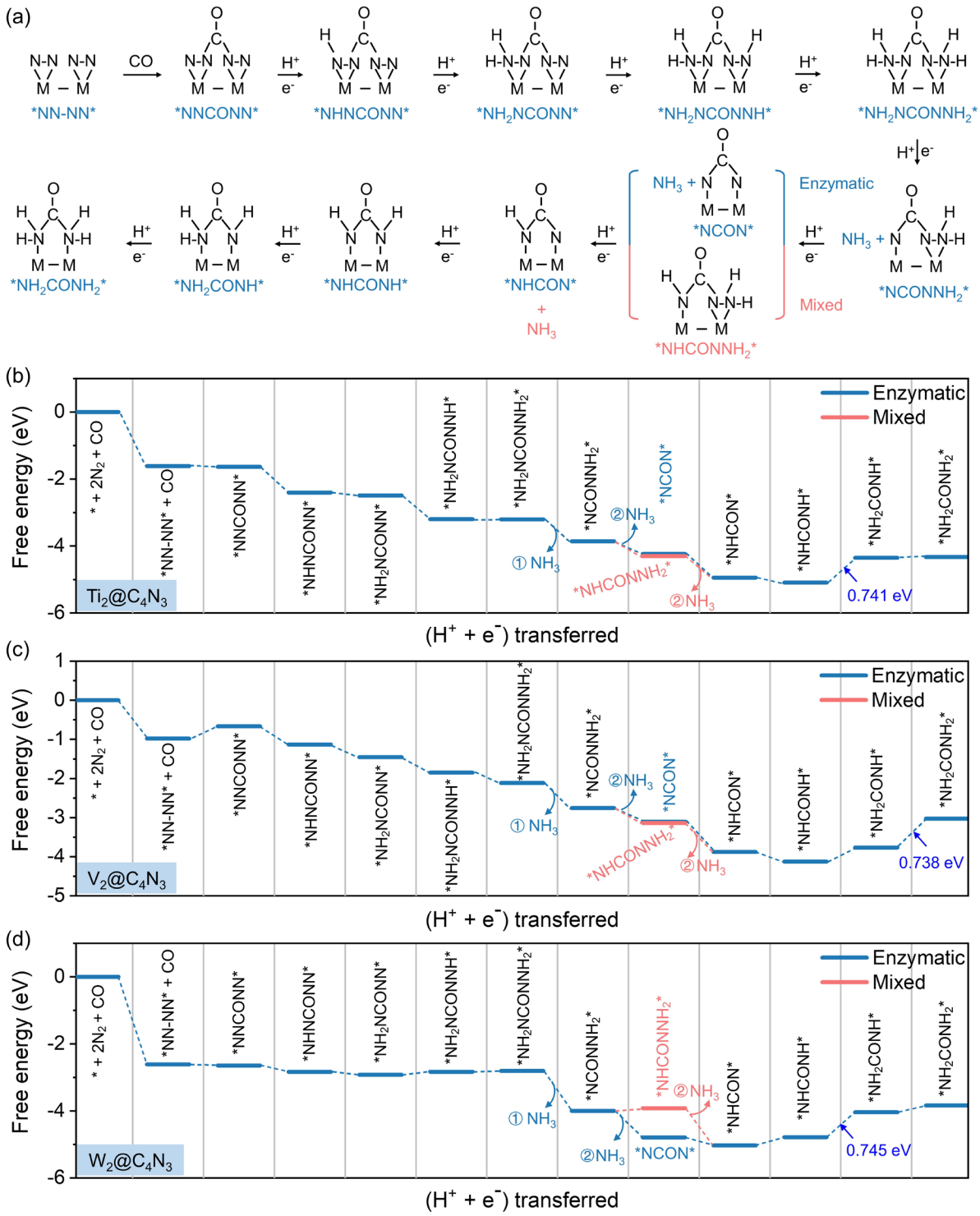

Figure 3. (a) Schematic diagram showing the completed mechanisms of urea formation via *N_2 dimerization and CO on $TM_2@C_4N_3$; Gibbs free energy diagrams for urea formation on (b) $Ti_2@C_4N_3$, (c) $V_2@C_4N_3$, and (d) $W_2@C_4N_3$, respectively.

2.3 Competition of C−N coupling and protonation

Although the proposed unique mechanism for the urea formation emphasizes the significance of

the *NNCONN* precursor, it is inevitable to generate the competitive *NHN-NN* (Figure S5) through the protonation step during the C−N coupling. To address this issue, the priority of C−N coupling and protonation after the adsorption of two N_2 molecules on $TM_2@C_4N_3$ (TM = Ti, V, Nb, and W) is further explored. As presented in Figure 4a, for $Ti_2@C_4N_3$, the Gibbs free energy change associated with inserting CO into the *NN-NN* is more negative than that of being hydrogenated to the intermediate *NHN-NN*, indicating the thermodynamic favorability of C−N coupling to form the *NNCONN* precursor. In the case of $V_2@C_4N_3$, it is found that the free energy changes for the formation of *NHN-NN* is slightly more favorable than that of *NNCONN*, which are 0.315 eV and 0.274 eV, respectively. However, when compared to the second protonation step of *NHN-NN* → *NH_2N-NN*, the formation of *NHNCONN* through the *NNCONN* → *NHNCONN* pathway is significantly more exothermic, as shown in Figure 4b, demonstrating the overwhelming dominance of direct C−N coupling on $V_2@C_4N_3$. As a comparison, Figure 4c displays that the *NHN-NN* intermediate on $W_2@C_4N_3$ is energetically more stable than *NNCONN*, whereas the C−N coupling can still occur via the *NHN-NN* → *NHNCONN* pathway, which exhibits a downhill energy profile (-0.089 eV) while the protonation step to form *NH_2N-NN* is endothermic (0.105 eV). Interestingly, our calculated results reveal that the ΔG of *NN-NN* →*NHN-NN* on $Nb_2@C_4N_3$ is -0.627 eV, which is two times lower than that of the *NN-NN* → *NNCONN*, indicating that the protonation is more preferred on $Nb_2@C_4N_3$ surface, as illustrated in Figure S6a. Nevertheless, it is noted that there is a severe distortion in the structure of *NHN-NN* on $Nb_2@C_4N_3$, where the nitrogen atom of the *NHN moiety bridges two Nb atoms (Figure S6a), suggesting a stronger interaction between Nb and N atoms. Such unexpected geometry of *NHN-NN* hampers the subsequent CO insertion, resulting in the exclusion of $Nb_2@C_4N_3$ from the further investigation.

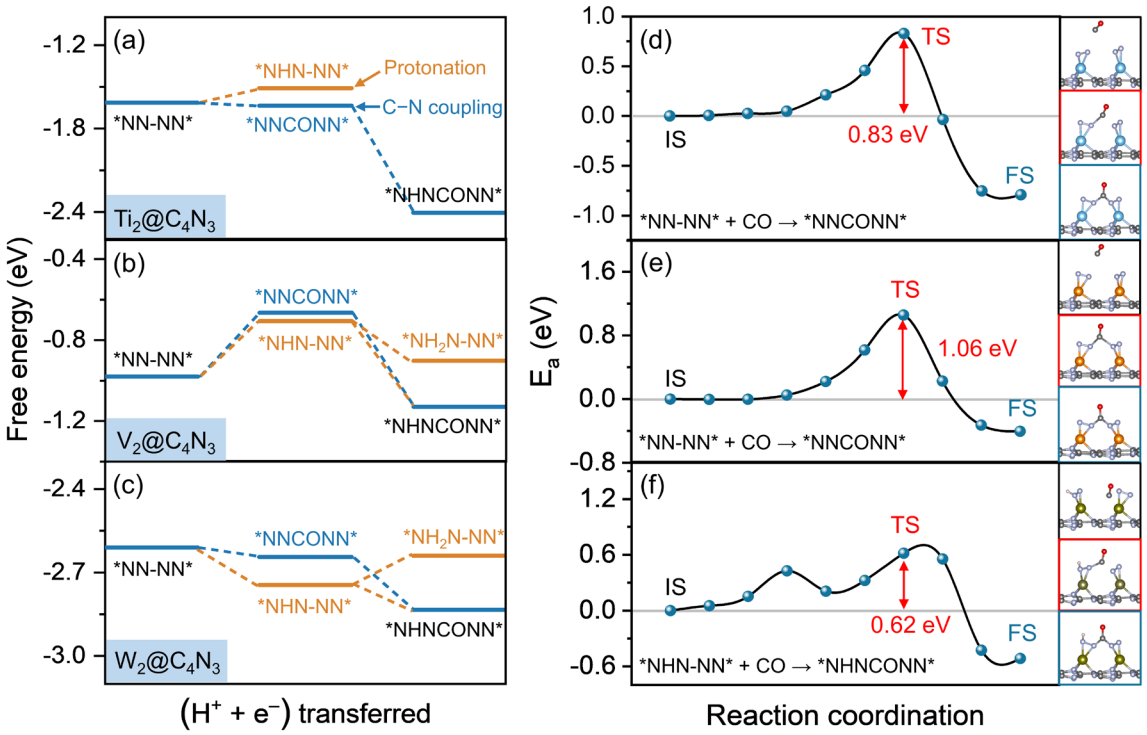

Figure 4. Competing C–N coupling and protonation step on (a) $Ti_2@C_4N_3$, (b) $V_2@C_4N_3$, and (c) $W_2@C_4N_3$, respectively; Kinetic energy barrier for C–N bond formation on (d) $Ti_2@C_4N_3$, (e) $V_2@C_4N_3$, and (f) $W_2@C_4N_3$, respectively. Insets are optimized structures in the initial (IS), transition (TS) and final states (FS) along the corresponding C–N bond formation pathway, respectively.

Except for the thermodynamic evaluation of the directly concurrent C–N coupling on $TM_2@C_4N_3$ (TM = Ti, V, and W), the kinetic feasibility is another indispensable factor to determine the catalytic activity for electrochemical urea production. Therefore, the kinetic energy barriers for N–C–N bond formation are assessed using the CI-NEB method, as shown in Figures 4d-f. The computed kinetic energy barrier (E_a) for C–N coupling through embedding the free CO molecule into the activated side-on *NN-NN* is 0.83 eV for $Ti_2@C_4N_3$ and 1.06 eV for $V_2@C_4N_3$, respectively, which are comparable to the PdCu alloy (0.79 eV)[14] and the MBenes catalysts (0.58–0.81 eV)[15], suggesting that the coupling of *NN-NN* and CO molecule in our proposed mechanism is kinetically feasible. As for $W_2@C_4N_3$, the calculated energy barrier for N–C–N bond formation via the protonated *NHN-NN* reacting with CO is 0.62 eV, which demonstrates the *NHN-NN* → *NHNCONN* pathway is also kinetically feasible. To confirm the robustness of the unique C–N coupling in forming the *NNCONN* or *NHNCONN* intermediate, we further conduct the kinetic evaluation of the traditional urea precursor

*NCON on $TM_2@C_4N_3$ (TM = Ti, V, and W). Usually, the formation of tower-like *NCON is sluggish because the insertion of *CO into $*N_2$ requires a high energy input to break the inert N≡N bond. Therefore, we calculate the energy barriers for N–N bond cleavage on $TM_2@C_4N_3$, as presented in Figure S7. It is evident that all energy barriers for breaking the N≡N bonds on $Ti_2@C_4N_3$, $V_2@C_4N_3$, and $W_2@C_4N_3$ are remarkably higher than those of the formation of *NNCONN* or *NHNCONN*, which indicates that the novel C−N coupling we proposed through $*N_2$ dimerization is kinetically more favorable compared to the conventional reaction pathway by directly breaking N≡N bonds.

2.4 Descriptor for electrochemical urea production

Based on our proposed mechanism, the man-power calculations of the reaction intermediates involved in the whole urea synthesis will consume massive computational resource for large-scale screening of every potential high-performance electrocatalyst. Therefore, it is paramount to uncover the structure–activity relationships by virtue of a specific descriptor. According to the previous reports, understanding the origin of intrinsic activity of different catalysts is crucial to the construction of descriptors, such as bonding network, local charges, and adsorption energy of the key intermediates.[36-39] However, these values heavily rely on the DFT calculations, making the large-scale screening and rational design of catalysts based on these features actually quite inefficient. Recently, Wang et al.[40] and Guo et al.[41] developed a simple descriptor Φ constructed by the inherent atomic properties of catalysts to predict the electrocatalytic performance of N_2 reduction reaction (NRR). Generally, the electron ‘‘acceptance and back-donation’’ mechanism has been widely recognized as the route for efficient activation of N_2 molecules,[42-44] thus, inspired by these studies, we assume that the distribution of d electrons of the TM atom should be the decisive factor to the $*N_2$ dimerization and subsequent C−N coupling as well as the reaction activity of urea synthesis. Herein, we for the first time introduce the descriptor Φ to describe the electrocatalytic activity of $TM_2@C_4N_3$ for urea production. This descriptor is defined as $\Phi = \frac{N_d}{\sqrt{\chi_{TM}/\chi_{sub}}}$, where N_d represents the number of d electrons; χ_{TM} and χ_{sub} are the electronegativities of the transition metal atom and substrate, respectively. This descriptor Φ can be understood as the effective d electron number. Here, χ_{sub} is defined as $(n\chi_N + m\chi_C)$, where χ_N and χ_C are the electronegativities of N and C atoms, respectively; n and m denote the numbers of N and C atoms

surrounding the TM atoms, respectively. $\sqrt{\chi_{TM}/\chi_{sub}}$ quantifies the effect of metal–support interaction on the TM's ability to attract electrons (more details can be found in Table S3). Notably, Figure S8 demonstrates a significant linear relationship between Φ and N_d, suggesting the validity of the proposed construction for the effective d electron number Φ.

As discussed above, the possible PDS of the whole $2N_2$ + CO co-reduction process on $TM_2@C_4N_3$ systems is derived from the last two hydrogenated intermediates of urea formation. To construct the activity map for urea synthesis, a three-step strategy is adopted for the activity evaluation. Specifically, reaction free energies for the C−N coupling (*NN-NN* + CO → *NNCONN*), the third (*NHCONH* + $H^+ + e^-$ → *NH_2CONH*), and last hydrogenation steps (*NH_2CONH* + $H^+ + e^-$ → *NH_2CONH_2*) for urea formation are calculated and the more positive one is adopted to obtain ΔG_L of the rate-limiting step. The calculated RLS and ΔG_L for all 3d, 4d, and 5d $TM_2@C_4N_3$ are listed in Table S4. Notably, it is found that $Zr_2@C_4N_3$ exhibits a good predicted electrocatalytic performance for urea synthesis, with the rate-limiting reaction of *NN-NN* + CO → *NNCONN* (ΔG_L = 0.762 eV). However, the *NNCONN* on $Zr_2@C_4N_3$ is thermodynamically unfavorable compared to the hydrogenated *NHN-NN*, as shown in Figure S6b, where *NHN-NN* shows a similar distortion to that observed in $Nb_2@C_4N_3$, leading to the removal from following analyses.

To prove our hypothesis, the relationship between the ΔG_L and the descriptor Φ is constructed, as shown in Figure 5a, where the volcano-type plot is obtained. The bi-linear relationships can be fitted as follows:

$-\Delta G_L = 0.10\Phi - 1.69$ (for $\Phi < 10.36$)

$-\Delta G_L = -0.15\Phi + 0.90$ (for $\Phi > 10.36$)

The strong linear correlation indicates that Φ can serve as a descriptor to evaluate the catalytic activity of $TM_2@C_4N_3$ for urea production from $2N_2$ + CO. The lowest ΔG_L and optimal activity for urea formation can be achieved for $TM_2@C_4N_3$ when Φ = 10.36, the screened catalysts $Ti_2@C_4N_3$, $V_2@C_4N_3$, and $W_2@C_4N_3$ sit at the apex of the "volcano" shape. These results are well consistent with the above activity calculations, indicating the effectiveness of the proposed descriptor. It is worth noting that the proposed descriptor Φ is merely composed of the inherent atomic properties including electronegativity

and d electron number that are available in the laboratory, allowing us to predict the activity of $TM_2@C_4N_3$ without any DFT calculation.

Except for the quantitative evaluation of urea production from $2N_2 + CO$ over g-C_4N_3-supported catalysts using the proposed descriptor Φ, our results also demonstrate a strong relationship between the adsorption energies of *NNCONN* ($\Delta E_{*NNCONN*}$) and *NCON (ΔE_{*NCON}), as depicted in Figure S9. Since the *NCON formed through the simultaneous N−N bond breaking and C−N bond coupling is the crucial intermediate in the conventional mechanism for urea formation from $N_2 + CO_2/CO$, the observed linear relationship in Figure S9 implies the potential universality of our proposed descriptor Φ. To confirm this, the data from reported electrocatalysts including $M_2@N_6G$,[38] MM'@N_6G,[38] PdCu alloy,[14] MBenes,[15] CuB_{12},[17] M/p-BN,[31] V_2N_6C,[45] MoP(111),[46] and CuPc[47] are collected and utilized to evaluate the relationships between the free energy change of rate-limiting step (ΔG_L) and Φ. As shown in Figure 5b and Table S5, the data points of reported catalysts are also in line with the established volcano relationship, indicating that the current descriptor is also applicable to traditional pathway for urea formation. The proposed descriptor Φ, which utilizes the intrinsic features of catalysts, can thus be adjusted and adapted to different substrate materials. This flexibility allows for quantifying the complicated interfaces, which holds promise for predicting the catalytic performance of urea formation.

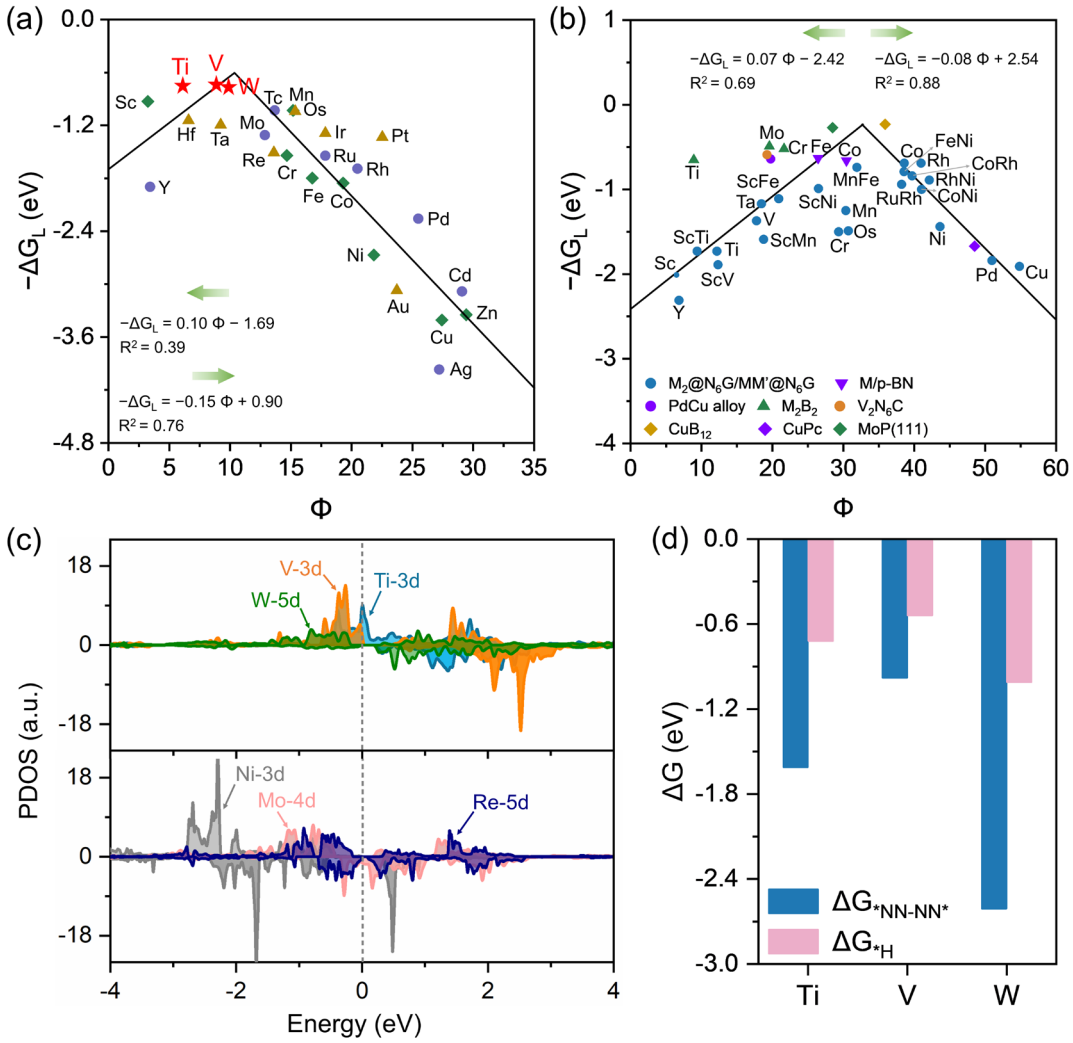

Figure 5. Volcano plot of ΔG_L versus the descriptor Φ for (a)$TM_2@C_4N_3$ and (b) reported catalysts [14-15, 17, 31, 38, 45-47]; (c) PDOS for d orbitals of Ti, V, Ni, Mo, W, and Re on $TM_2@C_4N_3$; (d) Gibbs free energy changes of *NN-NN* ($\Delta G_{*NN-NN*}$) and *H ($\Delta G_{*NN-NN*}$) for $Ti_2@C_4N_3$, $V_2@C_4N_3$, $W_2@C_4N_3$, respectively.

2.5 Activity origin and mechanism of $TM_2@C_4N_3$ towards urea production

Due to the high activity of the proposed C−N coupling mechanism, $Ti_2@C_4N_3$, $V_2@C_4N_3$, $W_2@C_4N_3$ have been identified as the promising electrocatalysts for urea production through N_2 dimerization. However, the activity origin of these catalysts is not yet clear. Generally, the intrinsic properties of the catalytic sites are essential to determine the adsorption energy of key intermediates and impact the catalytic performance. Therefore, the partial density of states (PDOS) of representative $TM_2@C_4N_3$ including Ti, V, W, Ni, Mo, and Re are focused and plotted in Figure 5c. According to the electron ‘‘acceptance and back-donation’’ mechanism,[42-44] the unoccupied d orbitals of TM atom can

accept the lone-electron pair and the occupied d-orbitals simultaneously donate electron into the anti-bonding orbitals of N_2 to weaken the N≡N bond. Figure 5c reveals that the number of anti-bonding orbitals of Ti, V, and W is adequate, and their bonding level are close to the Fermi level, which ensures the "acceptance-donation" interaction between the TM atoms and the reaction intermediates. As a comparison, the occupied orbitals of Ni, Mo, and Re are at deep levels and unoccupied orbitals are relatively fewer, leading to the ineffective adsorption and activation of reaction intermediates during urea production. Furthermore, the DOS of pure g-C_4N_3 without TM dopants has also been calculated, as shown in Figure S10. It is noteworthy that g-C_4N_3 exhibits a half-metallicity, with the spin-up state featuring a substantial bandgap of 2.18 eV, while no gap is observed in the spin-down channel, aligning with the previous reports.[48-49] Notably, it is found that the number of unoccupied orbitals in g-C_4N_3 is significantly lower than that of $TM_2@C_4N_3$ (TM = Ti, V, and W), indicating that effective doping with transition metals can indeed modify the electronic structures of g-C_4N_3.

2.6 Suppression of HER and stability of promising $TM_2@C_4N_3$

During the process of electrocatalytic ammonia and urea production, hydrogen evolution reaction (HER) is the main competitive reaction in aqueous solution, resulting in the decrease of faradaic efficiency. The selectivity between HER and $2N_2$ + CO co-reduction is determined via comparing the calculated free energy change of H adsorption (Volmer step) (Figure S11) of HER (ΔG_{*H}) with that of two N_2 molecules adsorption on $TM_2@C_4N_3$ (TM = Ti, V, and W), i.e., $\Delta G_{*NN-NN*}$. Figure 5d displays that all values of $\Delta G_{*NN-NN*}$ are more negative than those for ΔG_{*H}, which confirms that the $2N_2$ + CO co-reduction predominates over HER.

Additional to a high activity and excellent selectivity, eligible catalysts should be thermodynamically stable. To determine this, the thermodynamic stability of $TM_2@C_4N_3$ (TM = Ti, V, and W) are evaluated through the binding energy (E_b) and cohesive energy (E_{coh}),[50] which can be calculated by the following equations:

$$E_b = E_{TM_2@C_4N_3} - 2E_{TM} - E_{C_4N_3} \quad (1)$$

$$E_{coh} = E_{bulk} - 2E_{TM} \quad (2)$$

where $E_{TM_2@C_4N_3}$, E_{TM}, $E_{C_4N_3}$, and E_{bulk} represent the energies of $TM_2@C_4N_3$ catalyst, single TM atom,

C_4N_3 substrate, and metal bulk, respectively. All computed values of E_b and E_{coh} for $TM_2@C_4N_3$ (TM = Ti, V, and W) are summarized in Table S6, and negative E_b indicates that the adsorption of two TM atoms on g-C_4N_3 is thermodynamically favorable than being leached. Moreover, it is widely accepted that dispersed TM atoms are energetically more favorable than being aggregated when $E_b - E_{coh} < 0$.[51] Our calculated results show that the values of $E_b - E_{coh}$ are -3.153 eV for $Ti_2@C_4N_3$ and -2.141eV for $V_2@C_4N_3$, respectively, which suggests that embedding Ti and V atoms into the g-C_4N_3 substrate is energetically preferred than the metal aggregation. However, the cohesion of tungsten metal is significantly stronger than that of the binding ability of $W_2@C_4N_3$, resulting in a positive value of ($E_b - E_{coh}$), which implies undesirable thermodynamic stability of $W_2@C_4N_3$ candidate. Additionally, to further evaluate the thermal stability of the promising $Ti_2@C_4N_3$ and $V_2@C_4N_3$ catalysts, AIMD calculations at 500 K for 6000 fs are performed, as shown in Figure S12. The AIMD results reveal that $Ti_2@C_4N_3$ and $V_2@C_4N_3$ are kinetically stable at 500 K and the geometries are maintained after 6ps annealing, where the total energy and temperature fluctuate within small ranges. Therefore, it is demonstrated that g-C_4N_3 can firmly anchor the Ti and V atoms with high thermal stability, averting the issue of TM agglomeration.

In addition to the thermodynamic stability, qualified electrocatalysts should exhibit exceptional surface stability when exposed to electrochemical conditions. To determine this, the dissolution potential U_{diss}[31, 52-54] for the $Ti_2@C_4N_3$ and $V_2@C_4N_3$ was further computed to assess the dissolution-resistance of metal atoms from the substrate into water under an applied potential. Here, the U_{diss} is defined as

$$U_{diss} = U^{o}_{diss} - E_f/N_e \quad (3)$$

where U^{o}_{diss} is the standard dissolution potential of bulk metal, N_e is the number of electrons involved in the dissolution, and $E_f = 1/2\ E_b$ represents the formation energy of $TM@C_4N_3$, respectively. Generally, a catalyst is considered electrochemically stable when $U_{diss} > 0$ V. Our calculated results demonstrate that both $Ti_2@C_4N_3$ and $V_2@C_4N_3$ exhibit positive U_{diss} values of 2.09 V and 2.32 V, respectively, showcasing the excellent stability of $Ti_2@C_4N_3$ and $V_2@C_4N_3$ in electrochemical environments.

3. Conclusion

In conclusion, a new mechanism of electrocatalytic urea synthesis based on N_2 dimerization and CO is verified, and $TM_2@C_4N_3$ (TM = 3d, 4d, and 5d) catalysts are designed and screen by the DFT calculations. Among 28 candidates, $Ti_2@C_4N_3$ and $V_2@C_4N_3$ with high stability are singled out as the active and selective electrocatalysts for valuable ammonia and urea formation. The high activity and selectivity are attributed to the synchronously effective adsorption and activation of two N_2 molecules, which facilitates a direct C−N coupling without the toilsome N−N bond breaking. By this mechanism, the gaseous CO molecule preferentially inserts into *NN-NN* and binds concurrently with two N atoms, leading to the generation of symmetrical intermediate *NNCONN* served as the precursor for urea production. The low kinetic energy barrier for C−N coupling (0.83 eV for $Ti_2@C_4N_3$ and 1.06 eV for $V_2@C_4N_3$) together with low onset potential (-0.741 V for $Ti_2@C_4N_3$ and -0.738 V for $V_2@C_4N_3$) evidences the comparable catalytic performance to the benchmark PdCu alloy. Furthermore, effective d electron number (Φ) can be a simple but effective descriptor, which only consists of atomic characteristics (N_d, χ_{TM}, and χ_{sub}) to predict and design efficient electrocatalysts toward urea synthesis. More importantly, this proposed descriptor Φ can reproduce the order of reported activity in previous studies, suggesting the expansibility to evaluate the ΔG_L on other TM-doped catalysts. Our work not only verifies a novel mechanism for electrocatalytic urea formation, but also establishes a simple descriptor for rational design and rapid screening of optimal urea synthesis catalysts.

4. Computational Methods

All spin-polarized and periodic DFT calculations were performed using the Vienna Ab initio Simulation Package (VASP) code with projector-augmented wave pseudopotential (PAW).[55-57] The Perdew-Burke-Ernzerhof (PBE) functional at the generalized gradient approximation (GGA) level was employed to calculate the electron exchange-correlation energy.[58] The cutoff energy of the plane-wave basis was set to 520 eV, and the convergence criterion for the electronic self-consistent loop was 10^{-5} eV. The Brillouin zones were sampled using the Monkhorst-Pack mesh with a reciprocal space resolution of $2\pi \times 0.04$ Å^{-1} and $2\pi \times 0.02$ Å^{-1} for structural optimization and static self-consistent calculations, respectively. A Gaussian smearing was employed with a smearing width of 0.05 eV. A vacuum layer of 20 Å along the z-direction was applied to eliminate artifactual interactions between the

periodically repeated images. The DFT-D3 corrections were adopted for describing long-range van der Waals interactions here.[59-63] *Ab initio* molecular dynamic (AIMD) simulations were performed using the NVT ensemble at 500 K for 6 ps.[64] Atomic relaxations were carried out with the conjugate-gradient algorithm, until the Hellmann-Feynman forces were smaller than 0.01 eV/Å.

The computational hydrogen electrode (CHE) model proposed by Nørskov et al. was utilized to establish a free energy profile to describe the electrocatalytic performance of urea synthesis process.[65-66] The Gibbs reaction free energy change (ΔG) for each elementary step was evaluated from the equation:

$$\Delta G = \Delta E + \Delta E_{ZPE} - T\Delta S + \Delta G_U + \Delta G_{pH} \quad (4)$$

where ΔE is the total energy difference between the reaction intermediates and reactants, which can be directly obtained from DFT calculations; ΔE_{ZPE} and $-T\Delta S$ denote the changes in zero-point vibrational energy and entropy contribution at room temperature, respectively. Specifically, E_{ZPE} and TS of each reaction intermediate can be calculated by the following equations (2) and (3),[67-68] respectively:

$$E_{ZPE} = \frac{\sum_i h\nu_i}{2} \quad (5)$$

$$TS = RT\sum_i \left[\frac{h\nu_i}{k_B T}\frac{1}{e^{\frac{h\nu_i}{k_B T}} - 1} - \ln\left(1 - e^{-\frac{h\nu_i}{k_B T}}\right)\right] \quad (6)$$

where k_B represents the Boltzmann's constant, h is the Planck constant, ν_i denotes the frequency of the normal-mode of the adsorbed species, R is the ideal gas constant, and T is the system temperature, which is set to 298.15 K here. ΔG_U is the free energy contribution related to applied potential U, which can be obtained by the value of neU, where n is the number of transferred electrons and U stands for the operating electrochemical potential relative to the reversible hydrogen electrode (RHE). ΔG_{pH} is the correction of H concentration, i.e., $\Delta G_{pH} = k_B T \times \ln 10 \times pH$. In this work, the value of pH was assumed to be zero in a highly acidic solution.

The onset potential (U^{onset}) of the entire reduction reaction was obtained from the maximum free energy change of electron transfer steps, which is defined as:

$$U^{onset} = -\Delta G_{max}/e \quad (7)$$

where ΔG_{max} can be obtained from the most positive reaction free energy change during the whole process.

In addition, the activation energy barrier (E_a) was evaluated using the climbing image nudged

elastic band (CI-NEB) approach.[69-70] The convergence criteria for energy and force of geometry optimizations were set to 1×10^{-5} eV and 0.05 eV/Å, respectively. The minimum energy pathway (MEP) was examined using 8 images during the transition state search.

ASSOCIATED CONTENT

Supporting Information. The relationship between the *NN-NN* adsorption energy and *NNCONN* adsorption energy; Gibbs free energy diagrams for urea formation on $Cr_2@C_4N_3$, $Nb_2@C_4N_3$, $Mo_2@C_4N_3$, and $Tc_2@C_4N_3$; Side view of all optimized reaction intermediates in the whole process of $2N_2$ + CO co-reduction; Gibbs free energy diagrams for urea formation on $Ti_2@C_4N_3$ and $V_2@C_4N_3$ with solvent effects; Side view of optimized intermediates of *NHN-NN* and *NH_2N-NN*; Kinetic energy barrier for N–N bond breaking on $Ti_2@C_4N_3$, $V_2@C_4N_3$, and $W_2@$; The relationship between the descriptor Φ and number of d orbital electrons N_d; The relationship between the *NNCONN* adsorption energy and *NCON adsorption energy; Side view of the optimized *H intermediate; The variations of temperature and energy versus the time for AIMD simulations.

AUTHOR INFORMATION

Corresponding Author

Yuantong Gu − School of Mechanical, Medical and Process Engineering Faculty, Queensland University of Technology, Brisbane, QLD, Australia; orcid.org/0000-0002-2770-5014; Email: yuantong.gu@qut.edu.au

Liangzhi Kou − School of Mechanical, Medical and Process Engineering Faculty, Queensland University of Technology, Brisbane, QLD, Australia; orcid.org/0000-0002-3978-117X; Email: liangzhi.kou@qut.edu.au

Author

Junxian Liu − School of Mechanical, Medical and Process Engineering Faculty, Queensland University of Technology, Brisbane, QLD, Australia; orcid.org/0000-0002-5873-0095

Xingshuai Lv − Institute of Applied Physics and Materials Engineering, University of Macau, Macao SAR 999078, China.

Sean C. Smith − Integrated Materials Design Laboratory, Department of Materials Physics, Research School of Physics, The Australian National University, Australian Capital Territory, Canberra, ACT 2601, Australia.

Notes

The authors declare no competing financial interest.

ACKNOWLEDGMENTS

We acknowledge the grants of high-performance computer time from computing facility at the Queensland University of Technology. We also acknowledge the computational resources from the Pawsey Supercomputing Centre and Australian National Computational Infrastructure (NCI) which are allocated from the National Computational Merit Allocation Scheme supported by the Australian Government. Y.G. gratefully acknowledges financial support by the ARC Discovery Project (DP200102546). L.K. gratefully acknowledges financial support by the ARC Discovery Project (DP230101904).

REFERENCES

1. Erisman, J. W.; Sutton, M. A.; Galloway, J.; Klimont, Z.; Winiwarter, W., How a century of ammonia synthesis changed the world. *Nature Geoscience* **2008,** *1* (10), 636-639.
2. Comer, B. M.; Fuentes, P.; Dimkpa, C. O.; Liu, Y.-H.; Fernandez, C. A.; Arora, P.; Realff, M.; Singh, U.; Hatzell, M. C.; Medford, A. J., Prospects and Challenges for Solar Fertilizers. *Joule* **2019,** *3* (7), 1578-1605.
3. Volz, N.; Clayden, J., The Urea Renaissance. *Angewandte Chemie International Edition* **2011,** *50* (51), 12148-12155.
4. Liu, Y.; Zhao, X.; Ye, L., A Novel Elastic Urea–Melamine–Formaldehyde Foam: Structure and Properties. *Industrial & Engineering Chemistry Research* **2016,** *55* (32), 8743-8750.
5. Celleno, L., Topical urea in skincare: A review. *Dermatol Ther* **2018,** *31* (6), e12690.
6. Huang, H. M.; McDouall, J. J. W.; Procter, D. J., Radical Anions from Urea-type Carbonyls: Radical Cyclizations and Cyclization Cascades. *Angew Chem Int Ed Engl* **2018,** *57* (18), 4995-4999.
7. Seneque, M.; Can, F.; Duprez, D.; Courtois, X., NOx Selective Catalytic Reduction (NOx-SCR) by Urea: Evidence of the Reactivity of HNCO, Including a Specific Reaction Pathway for NOx Reduction Involving NO + NO2. *ACS Catalysis* **2016,** *6* (7), 4064-4067.
8. Krase, N. W.; Gaddy, V. L., Synthesis of Urea from Ammonia and Carbon Dioxide. *Journal of Industrial & Engineering Chemistry* **1922,** *14* (7), 611-615.
9. Meessen, J., Urea synthesis. *Chemie Ingenieur Technik* **2014,** *86* (12), 2180-2189.
10. Barzagli, F.; Mani, F.; Peruzzini, M., From greenhouse gas to feedstock: formation of ammonium carbamate from CO2 and NH3 in organic solvents and its catalytic conversion into urea under mild conditions. *Green Chemistry* **2011,** *13* (5), 1267-1274.
11. Service, R. F., New recipe produces ammonia from air, water, and sunlight. *Science* **2014,** *345* (6197), 610-610.
12. Licht, S.; Cui, B.; Wang, B.; Li, F.-F.; Lau, J.; Liu, S., Ammonia synthesis by N2 and steam electrolysis in molten hydroxide suspensions of nanoscale Fe2O3. *Science* **2014,** *345* (6197), 637-640.
13. van der Ham, C. J.; Koper, M. T.; Hetterscheid, D. G., Challenges in reduction of dinitrogen by proton and

electron transfer. *Chem Soc Rev* **2014,** *43* (15), 5183-91.
14. Chen, C.; Zhu, X.; Wen, X.; Zhou, Y.; Zhou, L.; Li, H.; Tao, L.; Li, Q.; Du, S.; Liu, T.; Yan, D.; Xie, C.; Zou, Y.; Wang, Y.; Chen, R.; Huo, J.; Li, Y.; Cheng, J.; Su, H.; Zhao, X.; Cheng, W.; Liu, Q.; Lin, H.; Luo, J.; Chen, J.; Dong, M.; Cheng, K.; Li, C.; Wang, S., Coupling N2 and CO2 in H2O to synthesize urea under ambient conditions. *Nat Chem* **2020,** *12* (8), 717-724.
15. Zhu, X.; Zhou, X.; Jing, Y.; Li, Y., Electrochemical synthesis of urea on MBenes. *Nat Commun* **2021,** *12* (1), 4080.
16. Roy, P.; Pramanik, A.; Sarkar, P., Dual-Silicon-Doped Graphitic Carbon Nitride Sheet: An Efficient Metal-Free Electrocatalyst for Urea Synthesis. *J Phys Chem Lett* **2021,** *12* (44), 10837-10844.
17. Zhu, C.; Wen, C.; Wang, M.; Zhang, M.; Geng, Y.; Su, Z., Non-metal boron atoms on a CuB12 monolayer as efficient catalytic sites for urea production. *Chem Sci* **2022,** *13* (5), 1342-1354.
18. Yuan, M.; Chen, J.; Xu, Y.; Liu, R.; Zhao, T.; Zhang, J.; Ren, Z.; Liu, Z.; Streb, C.; He, H.; Yang, C.; Zhang, S.; Zhang, G., Highly selective electroreduction of N2 and CO2 to urea over artificial frustrated Lewis pairs. *Energy & Environmental Science* **2021,** *14* (12), 6605-6615.
19. Zhang, N.; Jalil, A.; Wu, D.; Chen, S.; Liu, Y.; Gao, C.; Ye, W.; Qi, Z.; Ju, H.; Wang, C.; Wu, X.; Song, L.; Zhu, J.; Xiong, Y., Refining Defect States in W18O49 by Mo Doping: A Strategy for Tuning N2 Activation towards Solar-Driven Nitrogen Fixation. *Journal of the American Chemical Society* **2018,** *140* (30), 9434-9443.
20. Yuan, M.; Chen, J.; Bai, Y.; Liu, Z.; Zhang, J.; Zhao, T.; Wang, Q.; Li, S.; He, H.; Zhang, G., Unveiling Electrochemical Urea Synthesis by Co-Activation of CO2 and N2 with Mott-Schottky Heterostructure Catalysts. *Angew Chem Int Ed Engl* **2021,** *60* (19), 10910-10918.
21. Yuan, M.; Chen, J.; Bai, Y.; Liu, Z.; Zhang, J.; Zhao, T.; Shi, Q.; Li, S.; Wang, X.; Zhang, G., Electrochemical C-N coupling with perovskite hybrids toward efficient urea synthesis. *Chem Sci* **2021,** *12* (17), 6048-6058.
22. Norskov, J. K.; Abild-Pedersen, F.; Studt, F.; Bligaard, T., Density functional theory in surface chemistry and catalysis. *Proc Natl Acad Sci U S A* **2011,** *108* (3), 937-43.
23. Norskov, J. K.; Bligaard, T.; Rossmeisl, J.; Christensen, C. H., Towards the computational design of solid catalysts. *Nat Chem* **2009,** *1* (1), 37-46.
24. Liu, S.; Li, Z.; Wang, C.; Tao, W.; Huang, M.; Zuo, M.; Yang, Y.; Yang, K.; Zhang, L.; Chen, S.; Xu, P.; Chen, Q., Turning main-group element magnesium into a highly active electrocatalyst for oxygen reduction reaction. *Nat Commun* **2020,** *11* (1), 938.
25. Hong, W. T.; Risch, M.; Stoerzinger, K. A.; Grimaud, A.; Suntivich, J.; Shao-Horn, Y., Toward the rational design of non-precious transition metal oxides for oxygen electrocatalysis. *Energy & Environmental Science* **2015,** *8* (5), 1404-1427.
26. Zhong, W.; Qiu, Y.; Shen, H.; Wang, X.; Yuan, J.; Jia, C.; Bi, S.; Jiang, J., Electronic Spin Moment As a Catalytic Descriptor for Fe Single-Atom Catalysts Supported on C(2)N. *J Am Chem Soc* **2021,** *143* (11), 4405-4413.
27. Liu, K.; Fu, J.; Lin, Y.; Luo, T.; Ni, G.; Li, H.; Lin, Z.; Liu, M., Insights into the activity of single-atom Fe-N-C catalysts for oxygen reduction reaction. *Nat Commun* **2022,** *13* (1), 2075.
28. Ringe, S., The importance of a charge transfer descriptor for screening potential CO(2) reduction electrocatalysts. *Nat Commun* **2023,** *14* (1), 2598.
29. Zhang, X.; Wang, L.; Li, M.; Meng, W.; Liu, Y.; Dai, X.; Liu, G.; Gu, Y.; Liu, J.; Kou, L., Topological surface state: Universal catalytic descriptor in topological catalysis. *Materials Today* **2023**.
30. Jiao, D.; Wang, Z.; Liu, Y.; Cai, Q.; Zhao, J.; Cabrera, C. R.; Chen, Z., Mo2P Monolayer as a Superior Electrocatalyst for Urea Synthesis from Nitrogen and Carbon Dioxide Fixation: A Computational Study. *Energy & Environmental Materials* **2023**.
31. Kong, L.; Jiao, D.; Wang, Z.; Liu, Y.; Shang, Y.; Yin, L.; Cai, Q.; Zhao, J., Single metal atom anchored on porous boron nitride nanosheet for efficient collaborative urea electrosynthesis: A computational study. *Chemical Engineering Journal* **2023,** *451*.
32. Medford, A. J.; Vojvodic, A.; Hummelshøj, J. S.; Voss, J.; Abild-Pedersen, F.; Studt, F.; Bligaard, T.; Nilsson, A.; Nørskov, J. K., From the Sabatier principle to a predictive theory of transition-metal heterogeneous catalysis. *J. Catal.* **2015,** *328*, 36-42.
33. Hu, S.; Li, W.-X., Sabatier principle of metal-support interaction for design of ultrastable metal nanocatalysts. *Science* **2021,** *374* (6573), 1360-1365.
34. Mathew, K.; Sundararaman, R.; Letchworth-Weaver, K.; Arias, T. A.; Hennig, R. G., Implicit solvation model for density-functional study of nanocrystal surfaces and reaction pathways. *The Journal of Chemical Physics* **2014,** *140* (8), 084106.
35. Mathew, K.; Kolluru, V. S. C.; Mula, S.; Steinmann, S. N.; Hennig, R. G., Implicit self-consistent electrolyte model in plane-wave density-functional theory. *J Chem Phys* **2019,** *151* (23), 234101.
36. Ling, C.; Ouyang, Y.; Li, Q.; Bai, X.; Mao, X.; Du, A.; Wang, J., A General Two‐Step Strategy–Based High‐

Throughput Screening of Single Atom Catalysts for Nitrogen Fixation. *Small Methods* **2018,** *3* (9).
37. Li, H.; Liu, Y.; Chen, K.; Margraf, J. T.; Li, Y.; Reuter, K., Subgroup Discovery Points to the Prominent Role of Charge Transfer in Breaking Nitrogen Scaling Relations at Single-Atom Catalysts on VS2. *ACS Catalysis* **2021,** *11* (13), 7906-7914.
38. Zhu, C.; Wang, M.; Wen, C.; Zhang, M.; Geng, Y.; Zhu, G.; Su, Z., Establishing the Principal Descriptor for Electrochemical Urea Production via the Dispersed Dual-Metals Anchored on the N-Decorated Graphene. *Adv Sci (Weinh)* **2022,** *9* (10), e2105697.
39. Ren, Z.; Wang, X.; Wang, S.; Zhang, H.; Huang, B.; Dai, Y.; Wei, W., Efficient urea formation from N2O + CO on dual-atom catalysts TM2/g-CN. *Journal of Materials Chemistry A* **2023,** *11* (21), 11507-11516.
40. Fu, Z.; Wu, M.; Li, Q.; Ling, C.; Wang, J., A simple descriptor for the nitrogen reduction reaction over single atom catalysts. *Mater Horiz* **2023,** *10* (3), 852-858.
41. Niu, H.; Wang, X.; Shao, C.; Zhang, Z.; Guo, Y., Computational Screening Single-Atom Catalysts Supported on g-CN for N2 Reduction: High Activity and Selectivity. *ACS Sustainable Chemistry & Engineering* **2020,** *8* (36), 13749-13758.
42. Wang, S.; Shi, L.; Bai, X.; Li, Q.; Ling, C.; Wang, J., Highly Efficient Photo-/Electrocatalytic Reduction of Nitrogen into Ammonia by Dual-Metal Sites. *ACS Cent Sci* **2020,** *6* (10), 1762-1771.
43. Ling, C.; Niu, X.; Li, Q.; Du, A.; Wang, J., Metal-Free Single Atom Catalyst for N(2) Fixation Driven by Visible Light. *J Am Chem Soc* **2018,** *140* (43), 14161-14168.
44. Hu, R.; Li, Y.; Zeng, Q.; Wang, F.; Shang, J., Bimetallic Pairs Supported on Graphene as Efficient Electrocatalysts for Nitrogen Fixation: Search for the Optimal Coordination Atoms. *ChemSusChem* **2020,** *13* (14), 3636-3644.
45. Zhang, Z.; Guo, L., Electrochemical reduction of CO2 and N2 to synthesize urea on metal-nitrogen-doped carbon catalysts: a theoretical study. *Dalton Trans* **2021,** *50* (32), 11158-11166.
46. Jiao, D.; Dong, Y.; Cui, X.; Cai, Q.; Cabrera, C. R.; Zhao, J.; Chen, Z., Boosting the efficiency of urea synthesis via cooperative electroreduction of N2 and CO2 on MoP. *Journal of Materials Chemistry A* **2023,** *11* (1), 232-240.
47. Mukherjee, J.; Paul, S.; Adalder, A.; Kapse, S.; Thapa, R.; Mandal, S.; Ghorai, B.; Sarkar, S.; Ghorai, U. K., Understanding the Site‐Selective Electrocatalytic Co‐Reduction Mechanism for Green Urea Synthesis Using Copper Phthalocyanine Nanotubes. *Advanced Functional Materials* **2022,** *32* (31).
48. Du, A.; Sanvito, S.; Smith, S. C., First-principles prediction of metal-free magnetism and intrinsic half-metallicity in graphitic carbon nitride. *Phys Rev Lett* **2012,** *108* (19), 197207.
49. Bafekry, A.; Neek-Amal, M., Tuning the electronic properties of graphene–graphitic carbon nitride heterostructures and heterojunctions by using an electric field. *Physical Review B* **2020,** *101* (8).
50. Choi, C.; Back, S.; Kim, N.-Y.; Lim, J.; Kim, Y.-H.; Jung, Y., Suppression of Hydrogen Evolution Reaction in Electrochemical N2 Reduction Using Single-Atom Catalysts: A Computational Guideline. *ACS Catalysis* **2018,** *8* (8), 7517-7525.
51. Xu, H.; Cheng, D.; Cao, D.; Zeng, X. C., A universal principle for a rational design of single-atom electrocatalysts. *Nature Catalysis* **2018,** *1* (5), 339-348.
52. Guo, X.; Gu, J.; Lin, S.; Zhang, S.; Chen, Z.; Huang, S., Tackling the Activity and Selectivity Challenges of Electrocatalysts toward the Nitrogen Reduction Reaction via Atomically Dispersed Biatom Catalysts. *J Am Chem Soc* **2020,** *142* (12), 5709-5721.
53. Guo, X.; Zhang, S.; Kou, L.; Yam, C.-Y.; Frauenheim, T.; Chen, Z.; Huang, S., Data-driven pursuit of electrochemically stable 2D materials with basal plane activity toward oxygen electrocatalysis. *Energy & Environmental Science* **2023**.
54. Greeley, J.; Nørskov, J. K., Electrochemical dissolution of surface alloys in acids: Thermodynamic trends from first-principles calculations. *Electrochimica Acta* **2007,** *52* (19), 5829-5836.
55. Kresse, G.; Hafner, J., Ab initio molecular dynamics for liquid metals. *Physical Review B* **1993,** *47* (1), 558.
56. Kresse, G.; Furthmüller, J., Efficiency of ab-initio total energy calculations for metals and semiconductors using a plane-wave basis set. *Computational Materials Science* **1996,** *6* (1), 15-50.
57. Kresse, G.; Joubert, D., From ultrasoft pseudopotentials to the projector augmented-wave method. *Phys. Rev. B* **1999,** *59* (3), 1758-1775.
58. Perdew, J. P.; Burke, K.; Ernzerhof, M., Generalized Gradient Approximation Made Simple. *Phys. Rev. Lett.* **1996,** *77* (18), 3865-3868.
59. Grimme, S.; Antony, J.; Ehrlich, S.; Krieg, H., A consistent and accurate ab initio parametrization of density functional dispersion correction (DFT-D) for the 94 elements H-Pu. *J. Chem. Phys.* **2010,** *132* (15), 154104.
60. Dobson, J. F.; Gould, T., Calculation of dispersion energies. *J Phys Condens Matter* **2012,** *24* (7), 073201.
61. Bjorkman, T.; Gulans, A.; Krasheninnikov, A. V.; Nieminen, R. M., Are we van der Waals ready? *J Phys*

Condens Matter **2012,** *24* (42), 424218.
62. Dobson, J. F.; White, A.; Rubio, A., Asymptotics of the Dispersion Interaction: Analytic Benchmarks for van der Waals Energy Functionals. *Phys. Rev. Lett.* **2006,** *96* (7), 073201.
63. Sun, T.; Wang, Y.; Zhang, H.; Liu, P.; Zhao, H., Adsorption and oxidation of oxalic acid on anatase TiO2 (001) surface: A density functional theory study. *J Colloid Interface Sci* **2015,** *454*, 180-6.
64. Barnett, R. N.; Landman, U., Born-Oppenheimer molecular-dynamics simulations of finite systems: Structure and dynamics of $(H_2O)_2$. *Physical Review B* **1993,** *48* (4), 2081-2097.
65. Nørskov, J. K.; Rossmeisl, J.; Logadottir, A.; Lindqvist, L.; Kitchin, J. R.; Bligaard, T.; Jónsson, H., Origin of the Overpotential for Oxygen Reduction at a Fuel-Cell Cathode. *The Journal of Physical Chemistry B* **2004,** *108* (46), 17886-17892.
66. Valdés, Á.; Qu, Z. W.; Kroes, G. J.; Rossmeisl, J.; Nørskov, J. K., Oxidation and Photo-Oxidation of Water on TiO2 Surface. *The Journal of Physical Chemistry C* **2008,** *112* (26), 9872-9879.
67. Wang, Y.; Yuan, H.; Li, Y.; Chen, Z., Two-dimensional iron-phthalocyanine (Fe-Pc) monolayer as a promising single-atom-catalyst for oxygen reduction reaction: a computational study. *Nanoscale* **2015,** *7* (27), 11633-41.
68. Zou, X.; Wang, L.; Yakobson, B. I., Mechanisms of the oxygen reduction reaction on B- and/or N-doped carbon nanomaterials with curvature and edge effects. *Nanoscale* **2018,** *10* (3), 1129-1134.
69. Henkelman, G.; Jónsson, H., Improved tangent estimate in the nudged elastic band method for finding minimum energy paths and saddle points. *The Journal of Chemical Physics* **2000,** *113* (22), 9978-9985.
70. Henkelman, G.; Uberuaga, B. P.; Jónsson, H., A climbing image nudged elastic band method for finding saddle points and minimum energy paths. *The Journal of Chemical Physics* **2000,** *113* (22), 9901-9904.